



HAL
open science

Colloid dynamics near phase transition: A model for the relaxation of concentrated layers

Adriana Ferreira, Micheline Abbas, Philippe Carvin, Patrice Bacchin

► To cite this version:

Adriana Ferreira, Micheline Abbas, Philippe Carvin, Patrice Bacchin. Colloid dynamics near phase transition: A model for the relaxation of concentrated layers. *Colloids and Surfaces A: Physicochemical and Engineering Aspects*, 2022, 640, pp.128222. 10.1016/j.colsurfa.2021.128222 . hal-03929807

HAL Id: hal-03929807

<https://hal.science/hal-03929807>

Submitted on 13 Jul 2023

HAL is a multi-disciplinary open access archive for the deposit and dissemination of scientific research documents, whether they are published or not. The documents may come from teaching and research institutions in France or abroad, or from public or private research centers.

L'archive ouverte pluridisciplinaire **HAL**, est destinée au dépôt et à la diffusion de documents scientifiques de niveau recherche, publiés ou non, émanant des établissements d'enseignement et de recherche français ou étrangers, des laboratoires publics ou privés.

Colloid dynamics near phase transition: a model for the relaxation of concentrated layers

Adriana Ferreira^{a,b}, Micheline Abbas^{a,*}, Philippe Carvin^b, Patrice Bacchin^{a,*}

^a*Laboratoire de Génie Chimique, Université de Toulouse, CNRS, INPT,
UPS, Toulouse, France*

^b*Solvay, Research and Innovation Center of Lyon, Saint-Fons, France*

Abstract

The dynamics of concentrated colloidal dispersion close to a phase transition are challenging to predict. The presence of attractive interactions leads to hindered motions through the change in transport properties such as collective diffusion. We propose a continuum mechanical model to describe the dynamics of the relaxation of concentrated colloids near a phase transition. The model relies on a specific description of the equation of state of colloids, the osmotic pressure deriving from a free energy double-well function, that induces a decrease in collective diffusion close to the phase transition. The implementation of such transport properties in Computational Fluid Dynamics (CFD) codes enabled the description of a fast expansion of accumulated gels near an interface (induced for instance by evaporation or filtration processes) followed by a relaxation stage, where particles are progressively released from the layer toward the dilute bulk region. The model proposed in this work captures the increase of the relaxation time when approaching the transition, a feature of interest for engineering colloidal mixtures with concentration gradients.

Keywords:

*Corresponding authors

Email addresses: `adriana.bentescorreia@toulouse-inp.fr` (Adriana Ferreira), `micheline.abbas@toulouse-inp.fr` (Micheline Abbas), `philippe.carvin@solvay.com` (Philippe Carvin), `patrice.bacchin@univ-tlse3.fr` (Patrice Bacchin)

1. Introduction

The accumulation and relaxation of a concentrated colloidal phase is of interest in many applications, like drying and filtration, where out-of-equilibrium transport processes are encountered. A significant amount of experimental and theoretical works has focused on the accumulation of colloidal particles near an interface (a free surface and a solid membrane in the drying [1, 2], filtration [3] and pervaporation [4] configurations, respectively). However, there is evidence that concentration profiles, after the filtration is ceased, differ from those measured directly during filtration [5]. The dynamics and the mechanisms controlling the colloid relaxation (when colloidal compression is released) are far from being fully understood.

Colloidal particles can remain stable in a dispersed state for long durations, often due to repulsive electrostatic interactions or to the presence of certain stabilizing agents. When particle concentration increases in time, for instance, due to settling, drying or filtration, particles are compressed, which leads to the increase in osmotic pressure. The suspension can display non-equilibrium transition. The volume fraction at which phase transition occurs depends on the interactions between particles. When the concentration increases, particles are forced close to each other and attractive interaction forces become predominant. It is widely known that strongly attractive particles form gels at relatively low critical concentrations [6] (resulting from the formation of fractal clusters [7]), whereas weakly attractive particles form glass at high critical concentrations (permanent trapping of particles within cages formed by nearest neighbor particles) [8]. Nevertheless, colloidal dispersions with long-range electrostatic interactions can exhibit disorder-to-order transition, even at volume fractions as low as $\phi = O(0.1)$ [9, 10]. Once the concentration is sufficiently strong, networks of large numbers of particles are consolidated, leading the colloidal suspension to take the properties of a solid [11].

The equation of state of colloidal suspensions can exhibit sudden change near the phase transition [9, 12], leading to the dramatic slowing of the relaxation time-scales which manifests as a divergence in the local viscosity [13, 14] as hallmarks of liquid-solid transition [15]. These concentrated suspensions will be called gels hereafter. The properties of gels and their ability to relax is strongly related to inter-particle interaction (physico-chemical properties)

and to the temperature [16, 17, 18]. The experiments show that the relaxation of the gel occurs mainly by isotropic diffusion of the particles [19]. The objective of this work is to undertake a step forward toward the description of the relaxation process of a concentrated suspension, where the motion of particles is hindered by collective interactions close to phase transition. The description will be tackled with the aid of simple and realistic numerical simulations.

Numerical modeling allows studying the effect of physico-chemical colloidal interactions on the suspension dynamics, with the possibility to uncouple different effects when relevant [20]. This is typically the case for nanometric particles (like macromolecules or small particles) which exhibit gelation phenomena. The characteristic time and length scales corresponding to jelly material relaxation can be very large, compared to the scales corresponding to the diffusive motion of individual colloids, in a way that depends on physico-chemical properties [13]. Hence, the development of Eulerian numerical tools that enable the capture of these phenomena at macroscopic scale (by solving deterministic Partial Differential Equations to determine concentration field), including first order transitions (as it has been attempted for the gelation of colloids near a membrane [21]), are relevant for practical applications.

In order to study the gel layer relaxation at large length and time scales (compared to the colloid size and the associated diffusion time scale), we developed a tool that achieves a continuum description of the suspension concentration and motion. It is based on concepts from statistical mechanics (the Suspension Balance Model) [22]. In addition, the transport equations rely on the modeling of the colloidal properties that account for surface interactions: the cohesion of the matter that impacts the relaxation is related to inter-particle interactions. The osmotic pressure is a good way to account for local multi-body interactions between particles [23]. The advantage of using this property is two-fold. First, it can be easily accounted for in the frame of the continuous description, that enables the capture of the effect of local interactions at larger scales. Second, its dependence on the concentration (that represents the Equation Of State in the phase diagram) is experimentally accessible from the measurement of the suspension concentration at equilibrium in dialysis bags, or more recently, in microfluidic devices [24]. Osmotic pressure-based simulations have already proved that this approach

allows to detect how concentration polarisation can lead to gel or deposit formation during filtration [25] or to the formation of a skin layer during drying [26]. In that context a critical osmotic pressure was introduced, without the description of the equation of state during phase transition.

In this work, we develop an osmotic pressure model containing the essential ingredients to continuously describe the impact of inter-particle interactions on dispersion phase transition. The corresponding diffusion coefficient, deduced from the Stokes-Einstein generalized law, exhibits low values close to the irreversibility point. The diffusion model is used to perform simulations of concentrated colloids dynamics near phase separation i.e. for temperature, T , slightly above the critical temperature, T_c for phase separation ($\frac{T_c}{T} < 1$) in order to prevent phase separation from taking place. Simulations show that these properties can explain different relaxation kinetics of the accumulated layers according to the ratio $\frac{T_c}{T}$ that reflects the proximity to the instability zone and thus the irreversibility degree of the phase transition. In the following, section 2 describes the equation for colloid transport used for colloid accumulation and relaxation, while section 3 explains the background of the osmotic pressure model. The results displayed in section 4 demonstrate that such model of phase transition by osmotic pressure can describe the kinetics of relaxation of gel layers with a rapid gel expansion followed by a slow relaxation, this kinetics being controlled by the $\frac{T_c}{T}$ parameter.

2. Model based on hydrodynamic and thermodynamic concepts

The equation for colloid transport is first introduced, relying on a collective colloidal diffusion coefficient that depends on particle concentration $D(\phi)$. The relation between the diffusion coefficient and the osmotic pressure $\Pi(\phi)$ is thus introduced in the frame of the Stokes-Einstein generalized law. Second, a model of the osmotic pressure $\Pi(\phi)$, continuous over the entire volume fraction range, is proposed to account for reversible phase transition. Stars are used to refer to dimensionless quantities.

2.1. Colloid diffusion down a concentration gradient

The concentration of the colloidal particle phase will be described by the volume fraction ϕ that varies in space \mathbf{x} and in time t . The transport of

colloids in the solvent is based on the continuous description:

$$\frac{\partial \phi}{\partial t} = -\nabla \cdot \mathbf{J} \quad (1)$$

where \mathbf{J} denotes the colloid flux. In a suspension at rest, the colloid flux \mathbf{J} from higher to lower concentration regions originates from a thermodynamic force associated with the spatial gradient of chemical potential, and is counterbalanced by a solvent flux in the opposite direction, i.e. $\mathbf{J} = -D(\phi)\nabla(\phi)$. The diffusion of colloidal particles down a concentration-gradient, called collective diffusion, accounting for hydrodynamic and colloidal interactions can be expressed in the frame of the generalized Stokes-Einstein relation, to which thermodynamic and mechanical view points converge [27, 28]:

$$D(\phi) = \frac{K(\phi)}{6\pi\eta a} \frac{\phi}{1-\phi} \left(\frac{\partial \mu}{\partial \phi} \right)_{P,T} \quad (2)$$

$K(\phi)$ is the mobility function of a particle hindered by the presence of neighbor particles. The inverse of this mobility, i.e. the resistance function, valid across a wide volume fraction range is from Happel [29], $H(\phi) = \frac{1}{K(\phi)} = \frac{6+4\phi^{\frac{5}{3}}}{6-9\phi^{\frac{1}{3}}+9\phi^{\frac{5}{3}}-6\phi^2}$. The thermodynamic force responsible for collective diffusion is due to the gradient of the chemical potential per colloidal particle μ . The chemical potential variation with the concentration leads to a change in the osmotic pressure. This relationship can be written while neglecting the mixture compressibility:

$$\left(\frac{\partial \mu}{\partial \phi} \right)_{P,T} = V_p \frac{1-\phi}{\phi} \left(\frac{\partial \Pi}{\partial \phi} \right)_{\mu,T} \quad (3)$$

where Π denotes the osmotic pressure and V_p refers to the particle volume. Using eq. 3 in 2 and scaling the collective diffusion coefficient by the particle diffusion coefficient in the dilute limit $D_0 = \frac{kT}{6\pi\eta a}$ (where k and T correspond respectively to the Boltzmann constant and temperature), leads to:

$$D^*(\phi) = \frac{D(\phi)}{D_0} = \frac{1}{H(\phi)} \left(\frac{\partial \Pi^*}{\partial \phi} \right)_{\mu,T} \quad (4)$$

where D^* and $\Pi^* = \frac{V_p}{kT}\Pi$ denote the dimensionless diffusion coefficient and osmotic pressure, respectively.

In a more general situation, the flux \mathbf{J} can be written as the sum of a contribution induced by the mixture motion of the form $\phi\mathbf{u}_m$ and the contribution resulting from collective diffusion. Eq. 1 therefore takes the form:

$$\frac{\partial\phi}{\partial t} = -\nabla \cdot [\phi\mathbf{u}_m - D(\phi)\nabla\phi] \quad (5)$$

In a general configuration, the mixture velocity field \mathbf{u}_m can vary in space \mathbf{x} and time t , and should obey continuity and momentum conservation equations. In one-dimensional simulation, the mass conservation leads to constant mixture velocity u_m [30]. In a general framework, the transport equation (eq. 5) can be written in a dimensionless form, using the Péclet number that compares the transport by convection and diffusion, i.e. $Pe = U\delta/D_0$, where U is a characteristic mixture velocity and δ is a characteristic length scale for the concentration gradient. Since unidirectional mass transfer considered in this work lacks an imposed geometrical length scale (as explained later in section 4), the equations are maintained in their dimensional form. We draw the reader's attention to the fact that in the frame of the suspension balance model, the equation of particle transport can be written in another form, that evidences particle migration under the effect of mechanical forces arising from local variation in the osmotic pressure. Indeed, in the absence of external forces, the suspension balance model reflects the fact that spatial variation of osmotic pressure is counter-balanced by a drag force, i.e. $\phi\mathbf{F}_{drag} = V_p \frac{d\Pi}{d\phi} \nabla\phi$, that leads to particle slip with respect to the local mixture. This can be formulated by:

$$\frac{\partial\phi}{\partial t} = -\nabla \cdot \left(\phi\mathbf{u}_m - \frac{K(\phi)}{6\pi\eta a} \phi\mathbf{F}_{drag} \right) \quad (6)$$

The dual representation of the diffusive colloidal flux in eqs. 5 and 6 is very helpful to interpret dynamics of concentrated dispersed systems, whether colloidal or not [31, 32, 33]. This approach will allow us to further discuss the connection between the particle slip, with respect to the local mixture, and the diffusion strength.

2.2. Osmotic pressure near phase transition

Our main idea is to develop a model of the osmotic pressure $\Pi(\phi)$ property that include the effect of multibody colloidal interaction and of eventual

phase transition. First we shall briefly discuss the osmotic pressure and its dependence on the volume fraction. The equation of state of a colloidal system can be expressed in terms of osmotic pressure, which is defined, from the thermodynamic viewpoint, as the negative derivative of Helmholtz free energy with respect to volume at a constant temperature. In dilute systems, the main contribution to the osmotic pressure arises from the thermal fluctuation of colloids. As the concentration increases, inter-particle interactions (of interfacial and hydrodynamic origin) induce mechanical forces and consequently suspension mechanical pressure increases. The dependence of osmotic pressure on concentration is similar to that of water activity: the larger the colloid concentration, the higher is the energy required to extract additional water from the concentrated suspension. Available osmotic pressure-concentration isotherms accessible through direct or indirect methods (based on scattering), exhibit disorder-to-order phase transition signatures, as it has been shown in several experiments [9, 34, 12]. In order to obtain continuous solutions of practical mass transfer problems (by Eulerian simulation tools) in the frame of Stokes-Einstein generalized law, we construct a continuous and differentiable relationship for $\Pi(\phi)$ in a wide range of volume fractions including the transition range $\phi_1 < \phi < \phi_2$, .

We consider here that the phase transition occurs within a concentration range $\phi \in [\phi_1, \phi_2]$. By construction, the "critical volume fraction" is the arithmetic average of ϕ_1 and ϕ_2 , i.e. $\phi_c = \frac{\phi_1 + \phi_2}{2}$. The osmotic pressure is defined as the sum of two contributions defined in equations 8, 9 and 10, as following:

$$\Pi^* = \bar{\Pi}^* + \Pi_{tr}^* \quad (7)$$

Below the phase transition $\phi \leq \phi_c$: the osmotic pressure is described with classical virial expansion :

$$\bar{\Pi}^*|_{\phi \leq \phi_c} = \phi + C_2\phi^2 + C_3\phi^3 \quad (8)$$

The first term of the relationship represents the Van't Hoff law for ideal colloids (without specific interactions) and the other terms are Virial coefficients relative to the non-ideality induced by colloidal interactions. The second virial coefficient, C_3 , can describe the contribution of attractive interactions and, thus, a potential phase separation. However, this contribution is not sufficient to describe the colloid behavior over the complete range of

volume fraction.

Above the phase transition $\phi > \phi_c$: the osmotic pressure is defined by a relationship that diverges near the close packing volume fraction ϕ_{cp} :

$$\bar{\Pi}^*|_{\phi > \phi_c} = \bar{\Pi}^*(\phi_c) + \kappa \left. \frac{d\bar{\Pi}^*}{d\phi} \right|_{\phi_c} (\phi_{cp} - \phi_c) \left[\left(\frac{\phi_{cp} - \phi_c}{\phi_{cp} - \phi} \right)^{\frac{1}{\kappa}} - 1 \right] \quad (9)$$

The derivative of the main osmotic pressure contribution evaluated at the critical volume fraction is noted as $\left. \frac{d\bar{\Pi}^*}{d\phi} \right|_{\phi_c} = 1 + 2C_2\phi_c + 3C_3\phi_c^2$. The expressions of the main osmotic pressure contribution $\bar{\Pi}$ ensure its continuity and that of its first derivative at the critical volume fraction ϕ_c . The parameter κ in this equation represents the isothermal inverse compressibility of the condensed phase: high compressibility leads to a weak increase in osmotic pressure when increasing the volume fraction. Note that attributing some compressibility to dense layers of particles to account for established networks of connected particles can be commonly found in modeling of flocculated suspensions dewatering, although this is usually done through compressive yield stress [35, 36].

Close to the phase transition $\phi_1 < \phi < \phi_2$: an additional contribution to the osmotic pressure Π_{tr} originates from a double-well free energy, this approach being commonly adopted within the context of the phenomenological Cahn Hilliard equation [37] which takes into account the effect of attraction inducing the separation of the phases. The additional osmotic pressure can be written as :

$$\Pi_{tr}^* = 16 \left(\frac{T_c}{T} \right) \left. \frac{d\bar{\Pi}^*}{d\phi} \right|_{\phi_c} \frac{(\phi - \phi_1)^2(\phi - \phi_2)^2(\phi_c - \phi)}{(\phi_2 - \phi_1)^4} \quad (10)$$

This expression is built to satisfy the continuity of the equation of state and its first derivative along the entire range of accessible volume fractions. The transition does not change the value of the osmotic pressure, neither at ϕ_1 nor at ϕ_2 , in order to satisfy the Maxwell equal area rule (equilibrium between the different phase as seen in Fig.1). The main parameter of this model is $\frac{T_c}{T}$ that compares the temperature to the critical one at phase transition. This parameter allows the depth of the well energy to be scaled. We stress

here that the temperature should be understood as a concept that describes the system proximity to phase transition, and that eases the analogy with the first order gas-liquid phase transition. This will be explained further in section 3. Nevertheless, we note here that our model is inspired by the universal character of gel transition and its analogy with the vapor-liquid transition, as suggested by Tanaka [38] and modeled by Manning [39]. At high temperatures ($T \gg T_c$), $\frac{T_c}{T}$ tends to zero and the contribution of Π_{tr} to the global osmotic pressure is negligible. Said differently, there is no irreversibility in the system when the temperature is far from the spinodal phase separation. If $T = T_c$, the equation of state passes through the critical point and is tangent to the instability zone. At this point the osmotic pressure derivative is zero, leading to a negligible diffusion coefficient, i.e. irreversible transition. At low temperatures ($T < T_c$), the system loses its time reversal symmetry. An instability takes place, leading to phase separation of the suspension into highly concentrated regions (with aggregated or ordered particles) and regions depleted of particles. This situation corresponds to a negative derivative of the osmotic pressure, and thus gives rise to an apparent negative diffusion coefficient, as a hallmark of spinodal decomposition leading to demixing. Fig. 1 illustrates how the model (Eq. 7-10) can represent the equation of state with a typical variation near and inside the phase separation domain, based on different $\frac{T_c}{T}$ ratios.

In this paper, we investigate the effect of an abrupt decrease of the diffusion coefficient on the suspension relaxation when the system is close to phase transition without being subject to spinodal phase separation, i.e. only in the region where $\frac{T_c}{T} < 1$ in Fig. 1. In practice, this corresponds to situations where particles become ordered due to interactions with their neighbors, without being subject to irreversible aggregation, so that the mass transport equation (eq. 1) can be solved appropriately with a positive diffusion coefficient. Otherwise, if phase separation takes place, other classes of transport equations should be used, accounting for separated particle-rich and particle-poor regions.

3. Case study : Experiment-based osmotic pressure

Fig. 2 shows the evolution of the osmotic pressure as a function of the concentration of particles of diameter 10.2 nm, as obtained from the experimental work of Chang et al. [9]. The model explained in section 2 is applied here to describe the osmotic pressure of this experimental data, with the

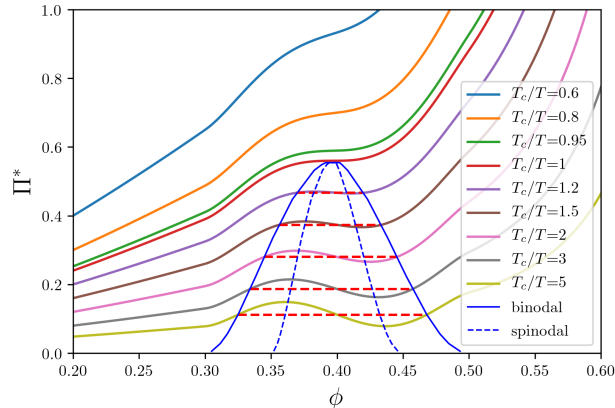


Figure 1: Equation of state – osmotic pressure - volume fraction isotherms for different $\frac{T_c}{T}$ ratios of 0.6, 0.8, 0.95, 1, 1.2, 1.5, 2, 3, and 5 corresponding to the blue, orange, green, red, purple, brown, pink, grey, and yellow lines, respectively. Spinodal decomposition (dashed line) occurs when the derivative of EOS is negative. $C_2 = 1, C_3 = 0, \phi_1 = 0.3, \phi_2 = 0.5, \kappa = 0.5$. Here ϕ_1 and ϕ_2 are assumed constant for simplicity.

following set of parameters to fit the data: $C_2 = 4 \times 10^4$, $C_3 = 15 \times 10^5$, $\kappa = 0.5$, $\phi_1 = 0.03$ and $\phi_2 = 0.09$. The different curves are obtained for different values of $\frac{T_c}{T}$ to illustrate the description of the transition zone between ϕ_1 and ϕ_2 . We pause here to explain the meaning of this parameter. The osmotic pressure measurements are realized at a given temperature and ionic strength (salt concentration). As the particle concentration is increased, the particles get closer to each other, leading to an increase in average potential energy. Below ϕ_1 , the average inter-particle distance remains greater than the repulsive barrier. However, above ϕ_1 , the distance can become less than this barrier. When the concentration falls to the transition range, the suspension undergoes metastable states, resulting in a change of the variation of the potential energy per particle with concentration [40]. This change in the potential energy depends on the value of the temperature compared to the critical temperature, which cannot be unambiguously measured from macroscopic measurements, as those realized by Chang et al. [9]. Therefore, $\frac{T_c}{T}$ is left as the parameter that represents the reversibility degree of the concentrated layers.

The collective diffusion coefficient obtained from eq. 4, which is based on the derivative of the osmotic pressure (Fig.2), is displayed in Fig.3 as a func-

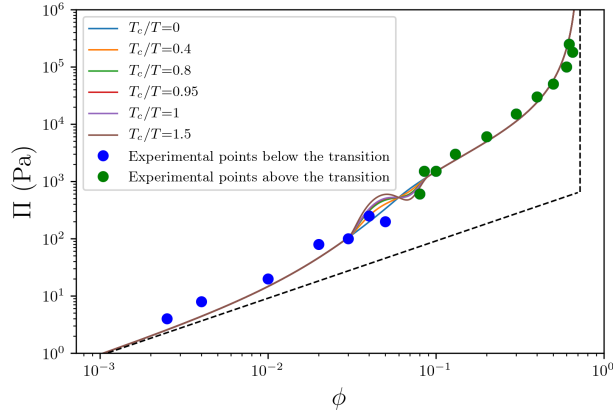


Figure 2: Modeling of osmotic pressure experimental data (blue and green symbols below and above the transition respectively) for silica [9]. The full line represent the fitting with the model for different $\frac{T_c}{T}$ ratios of 0, 0.4, 0.8, 0.95, 1 and 1.5 corresponding to the blue, orange, green, red, purple, and brown lines, respectively. The dashed line represents the limit of the Van't Hoff equation and the close packed volume fraction for dilute and concentrated dispersions respectively.

tion of the volume fraction, for different values of $\frac{T_c}{T}$ being always lower than 1 in order to avoid entering the unstable zone. The diffusion coefficient is independent of T_c/T for $\phi > \phi_2$ and $\phi < \phi_1$. Between ϕ_1 and ϕ_2 , a minimum of diffusion appears when the dispersion approaches the phase transition, this minimum being deeper and closer to zero when T is close to T_c . A very low diffusion coefficient (related to a plateau in osmotic pressure with volume fraction) is a hallmark of nearly arrested dynamics, where phase transition is approached: this has been demonstrated experimentally and theoretically [40, 41]. This behavior means that the mobility between concentrated and diluted phases close to the transition zone is negligible, i.e. the relative velocity of the phases associated with the drag force in Eq. 6 is zero, thus leading to slow dynamics [18, 42]. The low diffusion coefficient can be considered as a way to describe the dynamical arrest, which is a characteristic feature of colloidal gels or glasses [8]. Note that this minimum value of the diffusion coefficient occurs with two peaks below and above the critical volume fraction. This variation is the consequence of the osmotic pressure associated with a double-well energy function (Eq. 10) from which the diffusion coefficient is derived (through Eq. 4).

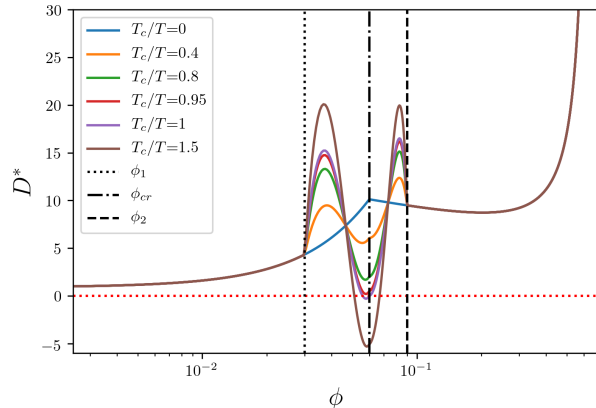


Figure 3: Variation of the diffusion coefficient as a function of the volume fraction for different $\frac{T_c}{T}$ of 0, 0.4, 0.8, 0.95, 1 and 1.5 corresponding to the blue, orange, green, red, purple, and brown lines, respectively. The minimum of the diffusion coefficient approaches zero when the temperature becomes close to the critical temperature. Vertical dotted, dot-dashed and dashed lines indicate the diffusion at ϕ_1 , ϕ_c and ϕ_2 , respectively.

4. Simulation of colloid relaxation

Simulations have been realized with the model presented in the previous section, by solving Eqs. 4, 5 and 7, in order to determine the relaxation of concentrated colloidal layers. Transient relaxation of colloidal suspensions displaying non-equilibrium phase transition are obtained from two initial conditions (Fig. 4). The first idealized situation corresponds to a colloidal film of uniform volume fraction ϕ_2 (Fig. 4a). This enables the discussion of the time required by a compacted suspensions to relax near phase transition, as a function of the system reversibility characterized by the parameter T_c/T . The second situation corresponds to a film accumulated near a membrane-like wall in order to mimic practical situations like gel formation during filtration or drying processes (Fig. 4b).

Equations 5, 4, and 7 are solved numerically using the open source software OpenFOAM (Open Field Operation and Manipulation) Foundation 7. In the present paper, the transport of colloids is restricted to one spatial direction (the y direction), assuming symmetry in other directions. The colloids are concentrated on one side (at low $y \rightarrow 0$), while the suspension is dilute at $y \rightarrow \infty$. Zero flux is imposed at the boundaries, i.e. $\frac{\partial \phi}{\partial y} = 0$

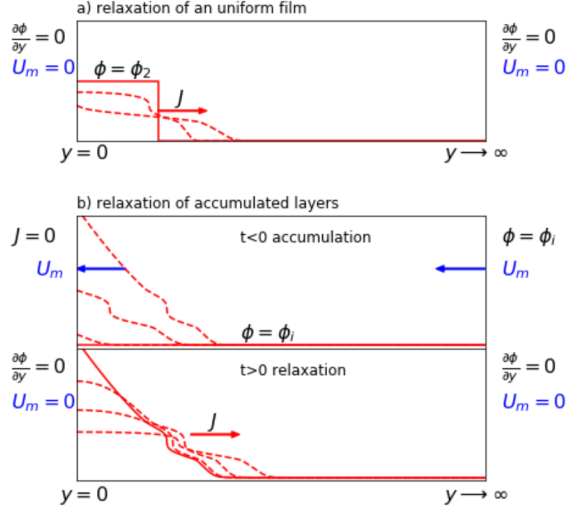


Figure 4: Illustration of the simulation procedures, with the plot of typical concentration profiles versus the wall-normal position y . Boundary conditions are given at $y = 0$ and $y \rightarrow \infty$. Two different situations are considered: a) Relaxation of an initially uniform film at $\phi_0 = \phi_2$ - b1) Colloid accumulation near a wall driven by a negative mixture velocity u_m (the different concentration profiles corresponding to different times), and b2) Relaxation of an accumulated film in a quiescent fluid. In the figures corresponding to the relaxation of colloidal layers, the starting concentration profiles are shown with red solid lines, while the transient 1D simulations are shown with dashed lines. The flux J of colloids leaving the concentrated layers is also sketched with red arrows.

at $y = 0$ and $y \rightarrow \infty$. The discretization of the divergence operator is performed using the "Gauss" discretization approach, and "Gauss linear" for the interpolation of the gradients. The Crank–Nicolson transient scheme is used for the discretization in time of the diffusion term. A fixed one-dimensional spatial grid with two regions is used. The first region ($0 < y < 1$) where the relaxation occurs contains 3200 cells with an expansion ratio of 100. Here l.u. denotes a numerical length unit in the simulation box. The second region ($1 < y < 20$ l.u.), used to mimic semi-infinite conditions, has 2000 cells with an expansion ratio of 20. The time step required to respect the Fourier stability criteria should be less than $\Delta y_{min}^2 / (2D_0)$, where the smallest mesh size is denoted as Δy_{min} (in our simulations the time step is 1×10^{-5}).

We draw the reader's attention that in the following sub-sections, the star (*) is used to indicate dimensionless time. The characteristic time scale is

inherently dependent on the configuration, i.e. accumulation or relaxation. For this reason, it will be mentioned explicitly in the figure captions.

4.1. Relaxation of an initially uniform film $\phi_0 \approx \phi_2$

We consider the relaxation of a uniform layer of initial concentration ϕ_0 and thickness δ_0 . Outside this layer, the bulk concentration is set to a small value ϕ_{bulk} (here we assume $\phi_{bulk} = 0$ without loss of generality). The colloid transfer from the layer to the bulk is thus set by $(\phi_0 - \phi_{bulk})$. In this case, the macroscopic length and time scales characterizing the relaxation of this layer are δ_0 and δ_0^2/D_0 , where D_0 is the particle diffusion coefficient in the dilute limit. As an example, if we consider the relaxation of a concentrated layer of thickness $100\mu m$ containing particles of diameter equal to $10nm$ in water at room temperature, the corresponding time scale is $\approx 500s$.

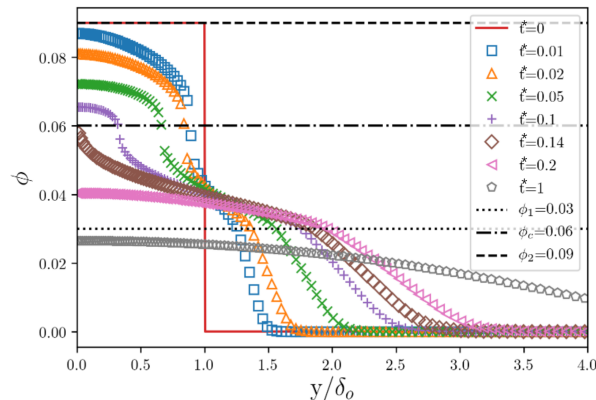


Figure 5: Relaxation of a uniform colloidal layer: wall-normal concentration profiles in time for $T_c/T = 0.95$. The profiles with the red line, blue squares, orange triangles, green crosses, purple plus, brown diamonds, pink left triangles, and grey pentagons are obtained at dimensionless relaxation times (scaled by δ_0^2/D_0) equal to 0, 0.01, 0.02, 0.05, 0.1, 0.14, 0.2, and 1 respectively. Horizontal dotted, dot-dashed and dashed lines indicate ϕ_1 , ϕ_c and ϕ_2 , respectively.

To study the colloid flow from the concentrated layer into the dilute bulk region, we have set $\phi_0 = \phi_2$. This is especially useful to describe the system relaxation when close to phase transition. In the absence of phase transition, the colloid diffusion down the concentration gradient progresses smoothly, like in a classic diffusion problem. Hence we focus on the dynamics close to

the critical point. The evolution in time of the wall-normal concentration profiles is shown in figure 5, for $T_c/T = 0.95$. At short times, this figure clearly identifies two different concentration gradients: a smooth gradient inside the suspension layer for $\phi < \phi_2$, and a steep gradient close to ϕ_c , where the particle release from the concentrated layer is reduced as the collective diffusion coefficient approaches small values. This extends the lifetime of the quasi-uniform layer near the wall. The flux of particles leaving the layer toward the dilute region leads to a reduction of the layer thickness. For larger times, once the layer concentration becomes less than the critical concentration, the evolution of the concentration profiles follows classic diffusion in a semi-infinite medium.

We stress here that, the closer the suspension to phase transition, i.e. $T_c/T \rightarrow 1$, the steeper the concentration variation at the layer front. A rigorous numerical solution of the problem would have required the use of an adaptative mesh, to finely resolve the transient steep-gradient region while the colloid layer shrinks. As our numerical scheme does not follow this procedure, and to avoid situations where numerical diffusion prevails over the physical diffusion, our study has been limited to systems where the minimum diffusion coefficient at ϕ_c is small, compared to $D(\phi_2)$, without approaching zero.

From the concentration profiles, we extracted a quantity that is of interest to applications, i.e. the amount of material that can potentially form a gel or glass (such that $\phi > \phi_c$). The thickness of the gel layer is called δ_g . In one dimension, this thickness is defined as $\delta_g = \int_{\phi > \phi_c} dy$. The corresponding mass of particles per unit area being $m_g = \rho_p \int_{\phi > \phi_c} \phi dy$. In order to characterize mass transfer of colloids from the dense layer toward the bulk, the decrease of δ_g over time was examined and is displayed in figure 6, where the film thickness is scaled by δ_0 and time by δ_0^2/D_0 .

During the early stages of film relaxation, the film thickness decreases like \sqrt{t} and the curves collapse, for any irreversibility parameter. This decrease corresponds to the particle diffusion from a layer where the diffusion coefficient is almost constant ($D(\phi_2)$) to a semi-infinite medium, initially at a constant concentration (equal to 0 in this case). After a short time, as the concentration varies across the film and the diffusion coefficient gradually decreases with y , it is not straightforward to theoretically predict the rate at

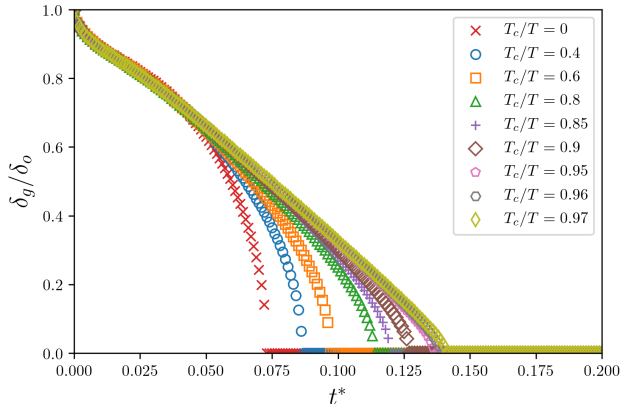


Figure 6: Evolution in time of the gel thickness δ_g , starting from a layer of thickness δ_0 of uniform concentration $\phi_0 = \phi_2$. The blue crosses, orange circles, green squares, red triangles, purple plus, brown diamonds, pink pentagons, grey hexagons, and yellow thin diamonds correspond to $T_c/T = 0, 0.4, 0.6, 0.8, 0.9, 0.95, 0.96$ and 0.97 , respectively. The gel thickness is scaled by the initial film thickness δ_0 and the time by δ_0^2/D_0 .

which δ_g decreases. From the simulations, the decrease of film thickness δ_g over time seems to follow a power law t^n , with a power $n > 1$ that depends on the irreversibility parameter. It is remarkable that the power tends to 1 when T_c/T approaches 1, or equivalently that the flux of particles leaving the dense layer is constant over time. Indeed, this is expected to be a consequence of the concentration jump at the interface between the dense layer and the bulk. The concentration jump is particularly steeper when the parameter T_c/T is close to 1. The particle flux at the so-called interface y_c can be obtained from $D(y_c) \frac{d\phi}{dy}|_{y_c}$. As $T_c/T \rightarrow 1$, while the diffusion coefficient $D(y_c)$ is small and the concentration gradient $\frac{d\phi}{dy}|_{y_c}$ is large, the resulting product seems to remain finite and constant during this second relaxation stage.

From the plot of the gel thickness δ_g over time, we defined the film relaxation time scale t_r as the time it takes for the maximum concentration in the layer to become less than ϕ_c . Said differently, this corresponds to the instance at which δ_g is canceled. Figure 7 shows t_r as a function of the irreversibility parameter T_c/T (here again, the time is scaled by δ_0^2/D_0). It can be clearly noticed that the relaxation time increases with the irreversibility parameter. When T_c/T approaches 1, we expect to observe the divergence

of this time scale, since particle release from the concentrated layer will be significantly hindered by the motion arrest near ϕ_c (at the layer front). Indeed, from eqs. 4 and 10 it can be inferred that the diffusion coefficient $D(\phi_c) \propto (1 - \frac{T_c}{T}) \frac{d\bar{\Pi}}{d\phi}|_{\phi_c}$, drops to small values especially when the suspension approaches the critical point. As the relaxation time of the particle layer by diffusive mass transfer is inversely proportional to the diffusion coefficient at the front of the layer, we expect the relaxation time to diverge like a power of $\frac{1}{1 - \frac{T_c}{T}}$.

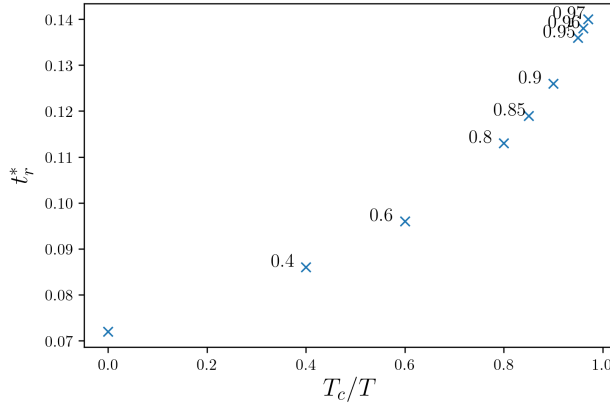


Figure 7: Relaxation time t_r^* (scaled by δ_0^2/D_0) of a uniform particle layer versus T_c/T .

4.2. Relaxation of an accumulated film

To simulate colloid accumulation near an interface (hereafter referred to as "wall") corresponding to evaporation or filtration processes, transport equation 5 has been solved with a constant (negative) wall-normal mixture velocity u_m (first step in Fig.4b). Far from the wall, the suspension is assumed to be sufficiently diluted, with a concentration $\phi_{bulk} < \phi_c$. During the accumulation stage, the pure fluid phase is allowed to evacuate through the wall located at $y = 0$ but not the particles. The zero particle flux J is ensured at the wall by setting the concentration gradient $\frac{d\phi}{dy}|_{y=0} = \frac{u_m}{D(\phi_w)}\phi_w$, where ϕ_w denotes the particle concentration at the wall. Note that the concentration gradient at the wall is negative as the mixture velocity u_m is negative, and that in this accumulation region, the particle velocity (of increasing concentration) is less than the fluid phase velocity, but the mixture velocity remains

constant along the y direction satisfying the mass balance. This behavior is consistent in the frame of the suspension balance formulation.

The particle accumulation near the wall is an infinitely transient process, where the thickness of colloidal layer grows continuously in time. Typical concentration profiles displayed in figure 8 result from the competition between particle accumulation by convection and opposite diffusion down the concentration gradient. $D_0/|u_m|$ and D_0/u_m^2 are the unique length and time scales during the accumulation: they will be called L_a and τ_a , respectively. L_a represents the characteristic thickness of the interface between the concentrated layer and the dilute suspension and τ_a characterizes the speed at which this front moves forward along the y direction. If we consider the filtration of particles of diameter $10nm$, at a typical filtration speed of $10^{-5}m/s$, $L_a = O(1)\mu m$ and $\tau_a = O(0.1)s$. Our model with the diffusion coefficient based on the osmotic pressure assumes that the time required for the colloids to reach thermodynamic equilibrium at a given concentration is less than the accumulation time scale τ_a . For a given irreversibility parameter, a unique representation of the concentration profiles during the accumulation stage takes the form $\frac{\phi}{\phi_0} \left(\frac{y}{L_a}, \frac{t}{\tau_a} \right)$.

During the colloid accumulation at the wall the concentration progressively increases as $y \rightarrow 0$. The exact shape of the concentration profile depends on the irreversibility parameter. Figure 8 displays the concentration profiles for three accumulation times, in the case where the suspension is close to phase transition, i.e. $T_c/T = 0.95$. As the diffusion coefficient drops significantly near phase transition at ϕ_c , a barrier is established near this concentration. The closer the system to the critical point (large T_c/T), the steeper the concentration jump. The jump in the concentration profile near the transition region is associated with a weak slip that the particles experience in this region. Indeed, the weak slip between the particle phase and the local mixture results from the small diffusion coefficient as ϕ approaches ϕ_c (as shown in eqs. 5 and 6). Once the particles cross this barrier, they fall in the dense region where the diffusion coefficient increases continuously with the concentration. When the concentration at the wall ϕ_w exceeds the transition range, the concentration profiles become self-similar. They exhibit a sharp variation in the transition region, and smoother variations in the concentrated and dilute regions. However, the concentration gradient is larger

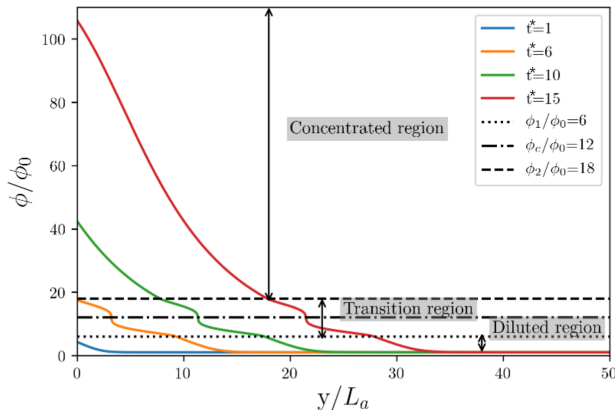


Figure 8: Concentration profiles obtained during particle accumulation at a wall, for different accumulation times (scaled by $1/\tau_a$) of 1, 6, 10, and 15 corresponding to the blue, orange, green, and red lines, respectively. The concentration ϕ is scaled by the bulk concentration ϕ_0 , while the position with respect to the wall is scaled by the characteristic accumulation length scale $L_a = D_0/|u_m|$. The irreversibility parameter is $T_c/T = 0.95$. Horizontal dotted, dot-dashed and dashed lines indicate ϕ_1 , ϕ_c and ϕ_2 , respectively.

in the concentrated region, where the diffusion coefficient is greater than in the dilute region (to give the reader a better idea, $D(\phi_2)/D(\phi_1) \approx 2.5$ for the particles considered in figure 3).

Next we examine the relaxation of the layers accumulated near the wall (second step in Fig.4b). At a given instant, the wall-normal velocity u_m is switched off, and the colloids are allowed to relax through the diffusion process. In this case, the characteristic length scale in the system is set by the thickness of the accumulated layer. While the shape and thickness of the film depend on the irreversibility parameter, we define a characteristic film thickness δ_c where the concentration is equal to the critical concentration ϕ_c . A sharp concentration gradient is observed near δ_c as $T_c/T \rightarrow 1$ (as observed in figure 8), while this jump is absent as $T_c/T \rightarrow 0$. At the onset of the relaxation, the position of the film where $\phi = \phi_c$ will be called δ_{c0} .

We consider for instance the relaxation of the green profile (in figure 8), where $\phi_w/\phi_0 \approx 40$, obtained at $t/\tau_a = 10$ for $T_c/T = 0.95$. At the onset of particle relaxation (resetting the initial time to $t = 0$) the film resulting from accumulation is geometrically separated in two phases. At $y > \delta_{c0}$,

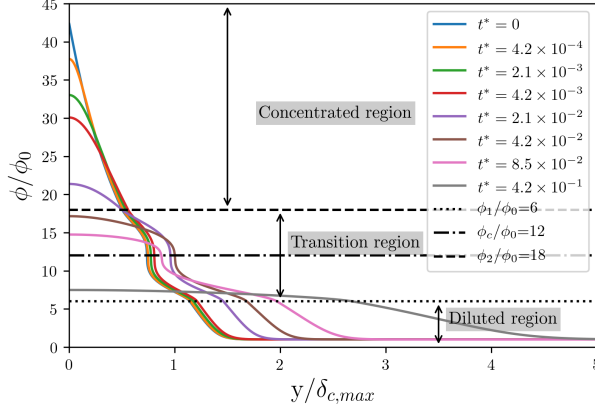


Figure 9: Relaxation of the accumulated colloidal film: wall-normal concentration profile in time for a $T_c/T = 0.95$ at different relaxation times $t^* = 0, 4.2 \times 10^{-4}, 2.1 \times 10^{-3}, 4.2 \times 10^{-3}, 2.1 \times 10^{-2}, 4.2 \times 10^{-2}, 8.5 \times 10^{-2},$ and 4.2×10^{-1} , corresponding to the blue, orange, green, red, purple, brown, pink, and grey lines respectively. The time is scaled by $\delta_{c,max}^2/D_0$. Horizontal dotted, dot-dashed and dashed lines indicate ϕ_1 , ϕ_c and ϕ_2 , respectively.

suspension behaves like a fluid phase where particles diffuse smoothly toward $y \rightarrow \infty$. However in the region falling near $y \approx \delta_{c0}$, the colloids are arrested as they exhibit very low diffusion coefficient in that region. The evolution of the concentration profiles in time is displayed in figure 9. The corresponding film thickness δ_g as a function of time is displayed in figure 10. As in figure 6, δ_g represents the thickness of the particle layer where the concentration exceeds ϕ_c . δ_g versus time is displayed for different irreversibility parameters T_c/T . Note that the initial state corresponding to all these curves is obtained separately, from the simulation of particle accumulation with different T_c/T parameters.

From figures 9 and 10, it can be observed that upon canceling the wall-normal (filtration or evaporation) velocity, the film relaxation exhibits two main stages, both of them being faster when the suspension is fully reversible, i.e. $T_c/T = 0$, as there is no real barrier against particle diffusion from the concentrated to the dilute region. During the first stage, in case the suspension is close to phase transition, the region of high concentration near the wall, subtended by the sharp front, quickly expands under the effect of high colloid diffusion or osmotic pressure. During this stage, the concentration

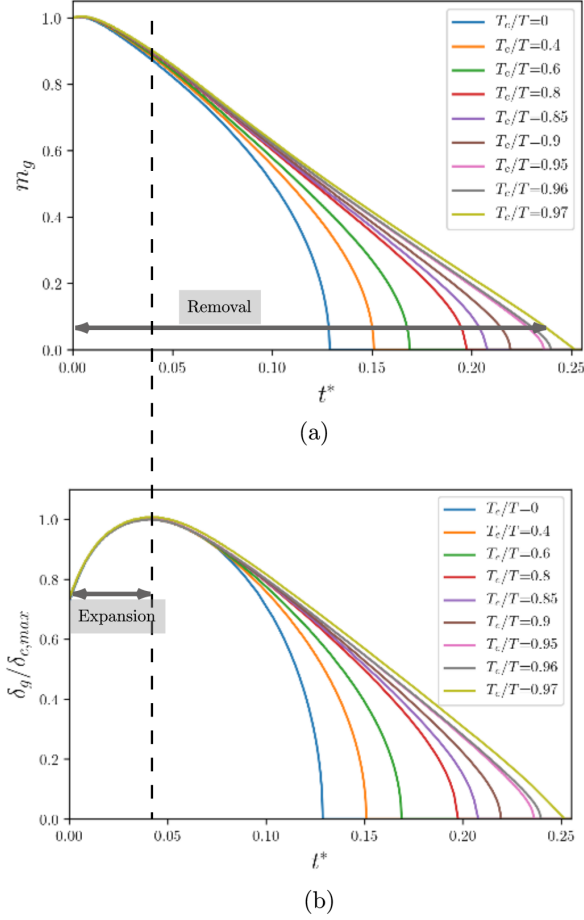


Figure 10: Evolution of (a) the mass of particles per unit area (scaled by the accumulated mass m_0 at the onset of relaxation) and (b) the gel thickness, during the relaxation stage for different irreversibility parameters $T_c/T = 0, 0.4, 0.6, 0.8, 0.85, 0.9, 0.95, 0.96,$ and 0.97 corresponding to the blue, orange, green, red, purple, brown, pink, grey, and yellow lines, respectively. The time is scaled by $\delta_{c,max}^2/D_0$. The concentration profile at the onset of the relaxation stage is taken after an accumulation time (scaled by t/τ_a) of 10.

gradient of the layer between the wall and the sharp front decreases significantly, without vanishing however (thus the decrease of film thickness as \sqrt{t} is not observed at the end of this stage). During a second stage, the colloid release from the near-wall layer is relatively slower, the kinetics being controlled by the irreversibility parameter. In the case $T_c/T \rightarrow 1$, the dynamics

during this stage is similar to that observed in the previous section, corresponding to the relaxation of a uniform particle layer (with $\phi = \phi_2$ at t_0). Indeed, the characteristic relaxation time scales are similar, and $\delta_g(t)$ tends to become linear as $T_c/T \rightarrow 1$.

Furthermore, the time t_r necessary to complete the relaxation of the accumulated layers is displayed in figure 11 as a function of the irreversibility parameter T_c/T . Here t_r corresponds to the time at which δ_g and m_g tend to 0. As the gel first expands before relaxing, the appropriate scaling for the time during the gel relaxation will be $\delta_{c,max}^2/D_0$, where $\delta_{c,max}$ corresponds to the characteristic film thickness of the gel at the end of the expansion stage (the maximum in figure 10b). This approximately allows the rationalization of the curve of the relaxation time as a function of the irreversibility parameter, when relaxation is considered starting from different accumulation profiles: the blue and orange symbols in figure 11 correspond to the relaxation of the green and red curves in figure 8, respectively. Indeed, the non-dimensional time for relaxation, starting from different accumulation conditions, are very close to each other confirming a good scaling law for the relaxation time.

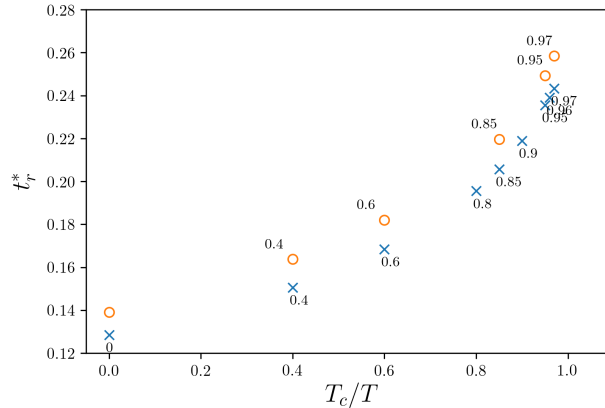


Figure 11: Relaxation time t_r^* as a function of the irreversibility parameter T_c/T of the non-uniform layers. The relaxation time is scaled by $\delta_{c,max}^2/D_0$, where $\delta_{c,max}$ corresponds to the maximum gel thickness at the end of the gel expansion stage. The blue crosses and orange circles are obtained from the relaxation of concentrated layers obtained at accumulation times (scaled by $1/\tau_a$) of 10 and 15, respectively.

By comparing figures 11 and 7, a similar trend for the evolution of the relaxation time required as a function of the irreversibility parameter can be observed. The fact that colloidal particles are arrested near phase transition retards the relaxation of a dense colloidal layer near a wall, and the relaxation time tends to diverge as the critical point is approached.

Notes on the results: We end this section by three remarks. First, we only considered in this work situations where the diffusion of colloidal particles is significantly reduced near the critical point, without allowing the suspension to undergo irreversible spinodal decomposition. Otherwise, this would require solving the interfacial dynamics between separated phases. Second, the osmotic pressure law assumes thermodynamic equilibrium. It is important to study whether this law holds true, when the colloidal suspensions is fully out of equilibrium, as is the case in this work. Third, the relaxation time scale computed in this work is qualitative. Indeed, the spatial grid was maintained fixed during particle accumulation and relaxation. Nevertheless, as the concentration jump near the singularity associated with colloidal arrest near ϕ_c is very steep, quantitative validation should be tested against advanced CFD tools that allow considering adaptative spatial discretization near the region where the singularity is located. These issues are open for future investigation.

5. Conclusion

This paper explores a model that can be used to study the dynamics of colloidal suspensions near phase transition. The model for colloid transport relies on the relationship between the colloid diffusion and osmotic pressure in the frame of the generalized Stokes-Einstein relationship, and can be implemented in the frame of any Eulerian CFD simulation tool. The osmotic pressure model accounts for first order transition near the critical point; the associated particle diffusion coefficient becomes very small when this parameter approaches 1. The model was applied to study the relaxation of a dense colloidal layer accumulated near an interface, subsequent to normal filtration or evaporation process. The suspension proximity to the critical point has been the main parameter of study, by means of a parameter T_c/T that describes the irreversibility degree of the phase transition. The simulations have shown that the film relaxation first undergoes an expansion stage where

the concentration in the layer decreases to the value ϕ_2 corresponding to the upper boundary of phase transition. The kinetics of particle relaxation is not dependent on the irreversibility parameter in this stage. During a second stage, a concentration jump subsists at the interface between the dense and dilute regions, especially when the local suspension state approaches the critical point. In this case, the particle release from the film is slowed down by the particle arrest near the critical point, leading to longer relaxation time scales.

The numerical simulations have shown that the relaxation time of a colloidal layer depends on both the irreversibility degree (associated with physico-chemical properties of transition) and the accumulated mass near an interface. In practice, based on our results, one can estimate the relaxation time from the gel mass as the following. After the gel expansion, the concentration is relatively equal to ϕ_2 , and the corresponding thickness of the gel phase $\delta_{c,max}$ can be estimated as the ratio $m_{g,0}/\phi_2$, where $m_{g,0}$ corresponds to the mass of the gel per unit area, accumulated near an interface, at the onset of relaxation. The relaxation time, in seconds, is then obtained from the dimensionless time displayed in figure 11 as $[t_r^* \times \delta_{c,max}^2/D_0]$. To conclude, the model and simulations shown herein constitute a first step toward the analysis of the variety of gel time relaxation data obtained with different experimental conditions as discussed in the introduction of this paper, and to characterize the relaxation dynamics with the T_c/T parameter.

Conflicts of interest

There are no conflicts to declare.

References

- [1] A. F. Routh, *Reports on Progress in Physics*, 2013, **76**, 046603.
- [2] P. Bacchin, D. Brutin, A. Davaille, E. Di Giuseppe, X. D. Chen, I. Gergianakis, F. Giorgiutti-Dauphiné, L. Goehring, Y. Hallez, R. Heyd *et al.*, *The European Physical Journal E*, 2018, **41**, 1–34.
- [3] P. Bacchin, A. Marty, P. Duru, M. Meireles and P. Aimar, *Advances in colloid and interface science*, 2011, **164**, 2–11.

- [4] N. Ziane and J.-B. Salmon, *Langmuir*, 2015, **31**, 7943–7952.
- [5] J. D. Sherwood, *AIChE J.*, 1997, **43**, 1488–1493.
- [6] J. Bergenholtz, W. C. K. Poon and M. Fuchs, *Langmuir*, 2003, **19**, 4493–4503.
- [7] A. Krall and D. Weitz, *Phys. Rev. Lett.*, 1998, **80**, 778.
- [8] V. Trappe and P. Sandkühler, *Curr. Opin. Colloid Interface Sci.*, 2004, **8**, 494 – 500.
- [9] J. Chang, P. Lesieur, M. Delsanti, L. Belloni, C. Bonnet-Gonnet and B. Cabane, *J. Phys. Chem.*, 1995, **99**, 15993–16001.
- [10] H. Tanaka, J. Meunier and D. Bonn, *Phys. Rev. E*, 2004, **69**, 031404.
- [11] R. Buscall and L. R. White, *J. Chem. Soc., Faraday Trans. I*, 1987, **83**, 873–891.
- [12] C. Pasquier, S. Beaufils, A. Bouchoux, S. Rigault, B. Cabane, M. Lund, V. Lechevalier, C. Le Floch-Fouéré, M. Pasco, G. Pabœuf *et al.*, *Phys. Chem. Chem. Phys.*, 2016, **18**, 28458–28465.
- [13] T. R. Kirkpatrick and D. Thirumalai, *Rev. Mod. Phys.*, 2015, **87**, 183–209.
- [14] J. G. Wang, Q. Li, X. Peng, G. B. McKenna and R. N. Zia, *Soft Matter*, 2020, **16**, 7370–7389.
- [15] G. L. Hunter and E. R. Weeks, *Reports on Progress in Physics*, 2012, **75**, 066501.
- [16] E. Del Gado and W. Kob, *Europhysics Letters (EPL)*, 2005, **72**, 1032–1038.
- [17] M. Doi, *Journal of the Physical Society of Japan*, 2009, **78**, 052001.
- [18] A. Di Biasio, *Colloids and Surfaces A: Physicochemical and Engineering Aspects*, 1998, **140**, 279–287.
- [19] Y. Yamagata and K. Miyamoto, *Colloids and Surfaces A: Physicochemical and Engineering Aspects*, 2021, **624**, 126786.

- [20] G. C. Agbanga, P. Bacchin and E. Climent, *Soft Matter*, 2014, **10**, 6303–6315.
- [21] P. Bacchin, B. Espinasse, Y. Bessiere, D. F. Fletcher and P. Aimar, *Desalination*, 2006, **192**, 74–81.
- [22] P. R. Nott and J. F. Brady, *J. Fluid Mech.*, 1994, **275**, 157–199.
- [23] L. C. Johnson and R. N. Zia, *Soft Matter*, 2021, **17**, 3784–3797.
- [24] H.-T. Nguyen, M. Massino, C. Keita and J.-B. Salmon, *Lab on a Chip*, 2020, **20**, 2383–2393.
- [25] P. Bacchin, D. Si-Hassen, V. Starov, M. J. Clifton and P. Aimar, *Chem. Eng. Sci.*, 2002, **57**, 77–91.
- [26] K. Ozawa, T. Okuzono and M. Doi, *Japanese journal of applied physics*, 2006, **45**, 8817.
- [27] G. Batchelor, *J. Fluid Mech.*, 1976, **74**, 1–29.
- [28] J. M. Schurr, *Chem. Phys.*, 1982, **65**, 217–223.
- [29] J. Happel, *AIChE journal*, 1958, **4**, 197–201.
- [30] P. Bacchin, *Colloids and Surfaces A: Physicochemical and Engineering Aspects*, 2017, **533**, 147–158.
- [31] M. Frank, D. Anderson, E. R. Weeks and J. F. Morris, *J. Fluid Mech.*, 2003, **493**, 363–378.
- [32] P. Bacchin, *J. Phys - Condens. Mat.*, 2018, **30**, 294001.
- [33] M. Abbas, A. Pouplin, O. Masbernat, A. Liné and S. Décarre, *AIChE J.*, 2017, **63**, 5182–5195.
- [34] A. Boire, P. Menut, M. H. Morel and C. Sanchez, *J. Phys. Chem. B*, 2015, **119**, 5412–5421.
- [35] K. A. Landman, C. Sirakoff and L. R. White, *Phys. Fluids A: Fluid Dynamics*, 1991, **3**, 1495–1509.
- [36] G. H. Meeten, *Colloid Surface A*, 1994, **82**, 77–83.

- [37] A. Novick-Cohen and L. A. Segel, *Physica D*, 1984, **10**, 277–298.
- [38] T. Tanaka, in *Phase Transitions of Gels*, ACS, 1992, ch. 1, pp. 1–21.
- [39] G. S. Manning, *ACS Omega*, 2018, **3**, 18857–18866.
- [40] J. C. F. Toledano, F. Sciortino and E. Zaccarelli, *Soft Matter*, 2009, **5**, 2390–2398.
- [41] Z. Varga and J. Swan, *Soft Matter*, 2016, **12**, 7670–7681.
- [42] L. Cipelletti and L. Ramos, *Journal of Physics: Condensed Matter*, 2005, **17**, R253.